Interannual variability of the upper ocean in the southeast Pacific stratus cloud region

Toshiaki Shinoda[1] and Jialin Lin[2]

[1]Naval Research Laboratory, Stennis Space Center, Mississippi

[2]Department of Geography, The Ohio State University, Columbus, Ohio

Corresponding author address

Toshiaki Shinoda
Naval Research Laboratory, Stennis Space Center, Mississippi, 39529
toshiaki.shinoda@nrlssc.navy.mil
Fax: 228-688-4759
Tel: 228-688-5356

Journal of Climate (in press)

April, 2009

Abstract

Persistent stratus/stratocumulus cloud decks in the southeast Pacific near the coasts of Peru and northern Chile play an important role in regional and global climate variability. Interannual variability of upper ocean under stratus cloud decks in the southeast Pacific is investigated using ocean general circulation model (OGCM) experiments. The model was first forced with daily surface fluxes based on the NCEP/NCAR reanalysis and satellite-derived surface shortwave and longwave radiation for the period of 1979-2004. Gridded surface heat flux estimates used in the model integration agree well with those based on WHOI IMET buoy measurements at 85°W, 20°S. Also, the OGCM is able to well reproduce observed interannual SST and sea surface height variations in this region. Our results suggest that the interannual variation of the upper ocean north of 20°S is mostly associated with ENSO variability. Additional model experiments were conducted to examine the relative importance of ocean dynamics and surface heat fluxes in determining the interannual variation in SST. The results of these experiments indicate that upper ocean dynamics play a dominant role in controlling the interannual variation of SST north of 20°S in the stratus cloud region. The upper ocean heat budget analysis shows that meridional heat advection associated with ENSO events primarily controls the interannual SST variation in the stratus cloud region north of 20°S

1. Introduction

The southeast Pacific near the coasts of Peru and northern Chile is characterized by persistent stratus/stratocumulus cloud decks that are important components of the complex coupled ocean-atmosphere-land system, and the variation of cloud decks has significant impacts on the global climate (e.g., Ma et al. 1996, Miller 1997, Gordon et al. 2000, Xie 2004). Stratus cloud decks have a substantial impact on the surface energy budget because of their high albedo (e.g., Lilly 1968, Schubert 1976, Li et al. 2002). In addition, stratus clouds could be responsible for the equatorial asymmetry of SST and winds in the eastern Pacific (e.g., Philander et al. 1996, Li 1997). Furthermore they may influence the seasonal cycle of SST in the eastern Pacific Ocean (e.g., Yu and Mechoso 1999, Fu and Wang 2001) and feed back on the El Nino Southern Oscillation (ENSO) cycle.

Air-sea coupled processes in this region are strongly influenced by the existence and variability of stratus clouds. Cloud decks shield incoming solar radiation, cooling the ocean, which helps to maintain the stratus clouds by stabilizing the lower troposphere. Thus, there is a positive feedback between the clouds and SST in this region (e.g., Norris and Leovy 1994, Klein et al. 1995). Accordingly, understanding the upper ocean processes that control SST in this region is crucial for simulating stratus clouds and thus predicting regional and global climate.

Until recently, there were few measurements of upper ocean and air-sea fluxes in the stratus deck region, which limited our ability to better understand and model the behavior of the atmosphere and ocean in this region. As part of the Eastern Pacific Investigation of Climate (EPIC) program, a surface mooring, which measures upper ocean temperature, salinity and velocity as well as surface meteorological variables, was deployed in the middle of stratus region (85°W, 20°S) in October 2000 (Colbo

and Weller 2007). While these mooring observations improved our understanding of upper ocean processes in this region, many issues remain unresolved. For example, stratus cloud decks cover a large area near the coast of Peru and Chile (∼10°S-30°S; e.g., Klein and Hartmann 1993, see also Fig.1 in Colbo and Weller 2007), and thus it is difficult to identify important upper ocean processes in the entire stratus region from the data obtained at one location. Also, the mooring data from October 2000 are not long enough to examine the interannual variation of the upper ocean in this region.

In this study, upper ocean processes associated with the interannual variation in the broad area of stratus decks are investigated using ocean general circulation model (OGCM) experiments. The data obtained from the mooring observations are utilized to validate the surface forcing fields used for the model integration and to evaluate the model performance. The OGCM experiments show that strong ENSO variability can influence the interannual SST variation in the southeast Pacific north of 20°S. Additional model experiments are performed to identify in detail the upper ocean processes that control interannual SST variation in this region. Also, the representativeness of the mooring observations at a particular location for broad-scale upper ocean variability in the stratus region is discussed based on the analysis of these OGCM experiments.

2. Model and control experiments

2.1 Model

The OGCM used in this study is the HYbrid Coordinate Ocean Model (HYCOM, Bleck 2002, Chassignet et al. 2003). The hybrid coordinate is isopycnal in the open, stratified ocean, but smoothly reverts to a terrain-following coordinate in shallow coastal regions, and to z-level coordinates in the mixed layer and/or unstratified seas. The K-Profile parameterization (KPP; Large et al. 1994) is used for vertical mixing in the model. Further details of the model are found in Bleck (2002).

The model domain covers the tropical Indo-Pacific basin, between 30°N and 40°S. A stretched horizontal grid is used to allow for increased resolution near the equator. The meridional grid spacing smoothly increases from 0.25° at the equator to about 1° at 30°N and 30°S. The meridional resolution between 30°S and 40°S is uniform 1°. The zonal grid resolution in the entire model domain is uniform 1°. 16 sigma (isopycnal) layers in the vertical with enhanced resolution in the upper ocean is chosen to better resolve the structures of upper-ocean currents and temperature fields, the thermocline, and the surface mixed layer. Because our focus is on upper ocean processes, σ_0 is used as a reference pressure. Open boundary conditions are employed along the northern and southern boundaries. It should be noted that the zonal grid resolution in the model is not sufficient to fully generate submesoscale eddies.

The model was first spun up using climatological forcing for 50 years from initial conditions based on climatological temperature and salinity (Levitus and Boyer 1994, Levitus et al. 1994). Then the model was integrated for two 26 year cycles (1979-2004), with the second cycle continuing from the end of the first cycle. The output with 3-day sampling for the 24-yr period (1981-2004) in the second cycle integration was analyzed. Hereafter, this experiment is referred to as “control experiment”.

2.2 Surface forcing fields and comparison with observations

The model was first forced with daily surface fluxes estimated from a combination of satellite data and the NCEP/NCAR reanalysis (Kalney et al. 1996) for the period 1979-2004. Surface shortwave and longwave radiation is obtained from the new satellite-based earth's radiation budget (ERB) data (referred to as ISCCP-FD hereafter) reconstructed by Zhang et al. (2004) available from July 1983-December 2006. Zhang et al. (2004) computed the radiation using a radiative transfer model along with the International Satellite Cloud Climatology Project (ISCCP) data. Radiation data from the NCEP/NCAR reanalysis are used before July 1983 for our model experiment.

Surface wind stress is estimated from daily winds at 10 m, specific humidity and air temperature at 2 m and SST from the NCEP/NCAR reanalysis utilizing a standard bulk formulae (Large and Pond 1981). Latent and sensible heat fluxes are calculated in a similar manner except using the model SST at each time step. Surface precipitation is obtained from Climate Prediction Center Merged Analysis of Precipitation (CMAP) pentad data (Xie and Arkin 1997), which are interpolated to daily resolution.

Previous studies have shown reasonable agreement between NCEP/NCAR surface meteorological variables (Serra et al. 2007) as well as surface fluxes calculated using NCEP/NCAR 10-m winds and in-situ and satellite-derived quantities (e.g., Shinoda et al. 1999). In this study, the accuracy of gridded surface flux estimates are evaluated by comparing them with those based on observations from the IMET mooring deployed at 85°W, 20°S in October 2000 (Colbo and Weller 2007; referred to as "IMET buoy data" hereafter). Surface fluxes of momentum and heat are computed from near surface meteorological variables measured at the IMET mooring (Colbo

and Weller 2007) using the TOGA COARE bulk flux algorithm (Fairall et al. 1996).

The IMET buoy was deployed every year in austral spring from October 2000. The first 4 datasets from each buoy (referred to as S1-S4 hereafter) are used to evaluate the gridded flux estimates in this study. Figure 1a shows time series of the daily mean surface shortwave radiation from the IMET buoy along with ISCCP-FD estimates from 19 October 2001-20 October 2002 (S2). The ISCCP-FD shortwave radiation agrees well with IMET observations (correlation coefficient: rr=0.82). The net surface heat flux from gridded data and the IMET estimates in the same period are shown in Fig. 1b. During this period, large subseasonal variations of surface heat flux are evident (see also Xu et al. 2005). The gridded net surface heat flux agrees well with the IMET estimates (rr=0.84) including the subseasonal variability. Zonal and meridional wind stresses estimated from IMET observations and gridded analyses are shown in Fig. 1c and 1d, respectively. These wind stresses also agree well with IMET estimates (rr=0.91 for the zonal stress, rr=0.87 for the meridional stress).

We have compared these flux estimates for all available years. The correlation coefficients, means and rms differences for the entire 4-year record are listed in Table 1. Correlations for the shortwave radiation, net surface heat flux and wind stress are similar to those found for S2 (Fig. 1), implying reasonable agreement of both annual and subseasonal variability. Also, the correlations for S1, S3, and S4 are similar to those for the entire 4-year record (not shown). The rms differences listed in Table 1 are comparable to those found during TOGA COARE (Shinoda et al. 1998). While the bias in the net surface heat flux ($\sim$30W/m^2) is much smaller than the magnitude of annual and subseasonal variability (Fig. 1), it is still significant and could impact the mean SST in the model. There is also a significant bias ($\sim$0.024N/m^2) in the meridional wind stress. The impact of these biases on upper ocean response is un-

known. These differences partly arise from the use of different bulk flux algorithms for the calculation of the surface flux quantities. A systematic study of model sensitivity to surface forcing fields in this region including the meridional wind stress and surface heat fluxes and its relation to air-sea feedback processes is part of our ongoing and future research.

In summary, surface fluxes of momentum and heat estimated from the NCEP/NCAR reanalysis and the ISSCP-FD data capture the variability observed at the IMET buoy site reasonably well. Although there are some discrepancies in the long-term mean values, the good agreement of surface flux variability between gridded estimates and those by Colbo and Weller (2007) suggests that the ISSCP-FD data, surface heat flux and the wind stress based on the NCEP/NCAR reanalysis are suitable for the present study. It should be noted that precipitation from CMAP does not agree well with that observed by the IMET buoy (not shown). Also, long records of sea surface salinity in this region are not available. Hence the variation of upper ocean salinity is not discussed in this paper. Further studies are required to examine the impact of the error in the surface freshwater flux on upper ocean dynamics.

It should also be noted that the diurnal cycle of shortwave radiation could impact longer time scale SST variability in the tropics (Shinoda and Hendon 1998, Shinoda 2005). However, the diurnal cycle primarily influences on intraseasonal time scales and the impact on SST variability of longer time scales is minimal (Shinoda 2005). Since this study focuses on interannual variability, the use of daily mean radiation should not be a major concern.

2.3. Control experiment

In this section, upper ocean variability in the control experiment is compared with that from the IMET buoy, and SST and SSH from the control experiment is compared

with satellite observations and the SST analysis (Reynolds et al. 2002; referred to as "Reynolds SST" hereafter). In addition, in order to establish the representativeness of the IMET mooring observations for broad-scale upper ocean variability in the stratus region, the interannual variations of SST and SSH at the IMET buoy site are compared with those for the entire stratus region using Reynolds SST and satellite-derived SSH.

a. Comparison with IMET observations

Model simulations using HYCOM were previously evaluated by comparing with in-situ and satellite observations (e.g., Shaji et al. 2005, Han 2005, Han et al. 2006, Shinoda et al. 2008). These studies indicate that HYCOM is able to simulate tropical upper ocean variability reasonably well.

Figure 2 shows the temperature in the upper 250 m during October 2001 - September 2002 (S2) from the control experiment and observations. Figure 3 is similar but for mixed layer depth and SST (Fig. 3a), as well as upper 50-m and 200-m heat content (Fig. 3b). The mixed layer depth is defined as the depth at which density increases by Δd above the surface value. Here, Δd is specified to be equivalent to the density increase produced by a 0.5°C decrease in temperature from the surface value, but with the salinity held constant at the surface value. These comparisons suggest that the model is able to well capture the seasonal evolution of the mixed layer. During austral summer (January-February), the mixed layer depth is about 50 m. The deepening of the mixed layer occurs during fall and winter. The deepest mixed layer is observed in the September-October season, which is $\sim$160-180 m. Despite the overall good agreement, there are some significant differences between the observed and the model mixed layer depth during November-December ($\sim$50m). These differences could partly be attributed to the spatial variation of mixed layer

depth around the IMET site on the scale that cannot be resolved by gridded surface fluxes. These results may also suggest a deficiency in the surface fluxes used to force the model and/or an inability of the model to fully represent upper ocean mixing processes.

The seasonal SST variation associated with the mixed layer evolution is also well simulated by the model. The warmest SST of ∼24°C is observed in mid-March, and it then decreases as the mixed layer deepens. The coldest SST of about 18.5-19°C is found in late September to early October. The mean SST during this period from the model and observation is 20.89°C and 20.44°C, respectively. The seasonal evolution of the mixed layer and SST is similar in other years (see Fig. 3 in Colbo and Weller 2007), and is simulated by the model reasonably well (not shown).

While the seasonal evolution of mixed layer depth and SST are reasonably well simulated by the model, there are significant discrepancies below 150 m between the model and observations. The vertical temperature gradient in the thermocline is much larger (sharper thermocline) in the observations than in the model. Thus, while the heat content of the upper 50 meters in the model and the observations is similar, the upper 200 meter heat content in the model is significantly larger. These errors in the thermocline structure below 150 m in the tropical oceans are found in other OGCMs, and improvements of temperature structure at this depth range awaits further development of mixing parameterization (e.g., Yu and Schopf 1997). Nevertheless, the model reproduces the seasonal evolution of SST and mixed layer observed at the IMET buoy site reasonably well, and thus it provides a tool for examining longer time scale variability of the upper ocean in this region.

b. Interannual variability

The model upper ocean variability in the stratus region for the entire analysis period (1981-2004) is compared with that from satellite altimeter measurements and Reynolds SST to validate the model performance on interannual time scales. Figure 4a displays the time series of SST anomalies at 85°W, 20°S from the model and Reynolds SST. Anomalies are computed by subtracting the annual cycle (first three harmonics of the seasonal cycle). The annual mean SST from the model and Reynolds SST are 20.9°C and 20.4°C, respectively. Prominent interannual variations of SST are evident in both model and observations however they are notably smaller during the period of IMET observations. Interannual SST variability at this site is reasonably well simulated by the model (rr=0.7), however, there are some notable differences. For example, the model underestimates the large warming during 1982/83 by ∼1°C.

In order to examine the representativeness of the IMET buoy site for broad-scale upper ocean variability, interannual SST variations north and south of the mooring site are also investigated. Figure 4b shows the time series of SST anomalies averaged over the area 90°W-80°W, 20°S-10°S, just north of the IMET buoy site. The annual mean SST from the model and Reynolds SST for this region are 22.4°C and 21.6°C, respectively. Again, large interannual variations are evident in both time series. The agreement between the model and Reynolds SST is significantly better (rr=0.87). Also, the time series are similar to ENSO indices (e.g., Nino3 SST). Large warming is observed during only the major El Nino events (1982/83, 1987, 1991-92, 1997/98), which is significantly different from that at the IMET site.

Figure 4c displays the time series of SST anomalies averaged over the area 90°W-80°W, 30°S-20°S, just south of the IMET buoy site. The annual mean SST from the model and Reynolds SST in this region are 20.4°C and 19.8°C, respectively. In

contrast to Fig. 4b, significant ENSO signals are not found in this region, and SST variability on shorter time scales (∼4-9 months) is often observed. The large warming during 1992-93 observed at 85°S, 20°S is also found in this area. The model is able to well simulate these SST variations.

In order to further investigate the prominent interannual warming events at the IMET site, the spatial variation of SST during each warming is examined using Reynolds SST. Figure 5a shows the SST map during November 1997 from the SST analysis when the large warming at the IMET site is observed. The IMET site is located at the southern edge of ENSO influence that causes significant warming during this period (see also Kessler 2006). However, the large warming at the IMET site during January 1992 is not the direct influence of ENSO (Fig. 5b), in which the maximum SST is located south of 20°S. While the IMET site is located at the southern edge of ENSO influence, other significant SST changes originating from south of the buoy site also influenced the interannual SST variation. It should be noted that the model is able to simulate the spatial variation of these warming events reasonably well (not shown). It should also be noted that a similar SST pattern is observed during September-November 1982 in which the maximum SST is located south of 20°S (not shown). The model is not able to simulate this warming during this period (Fig. 4c). The reason for this is unknown. However, a deficiency in shortwave radiation from the NCEP reanalysis could contribute to this SST error since ISCCP-FD radiation is available only from July 1983.

In order to validate the dynamical ocean response in the model, sea surface height (SSH) anomalies are also compared with those from the ocean TOpography Experiment (TOPEX) data. TOPEX SSH data, available as 10-day means, are first linearly interpolated to daily values. The monthly average is then computed from the daily values. Anomalies are computed by subtracting the annual cycle during the

period 1992-2002. Figure 6 shows the monthly time series of SSH from the model and TOPEX during the period 1992-2002, when the TOPEX data are available. The model is able to well capture the interannual variation at the IMET site (rr=0.72; Fig. 6a). The correlation is better for the area average of 80°W-90°W, 10°S-20°S (rr=0.90; Fig. 6b). During this period, the time series are dominated by the 1997/98 El Nino event. The amplitude and timing of the onset and demise of this El Nino are captured by the model very well. SSH anomalies south of the IMET buoy site (80°W-90°W, 20°S-30°S) are shown in Fig. 6c. Although the interannual variation is much smaller than that in Fig. 6b, the model is able to well simulate the observed SSH. The good agreement of the model with both SST and SSH data suggests that it is worthwhile to conduct further experiments to examine upper ocean processes associated with the interannual SST variation in this region.

3. Relative importance of ocean dynamics and surface heat flux

The analysis of Reynolds SST in the previous section indicates that the interannual SST variation is largely influenced by ENSO only north of 20°S. Also, our comparisons with observations indicate that the model is able to simulate interannual SST and SSH variations very well. In this section, a series of model experiments are analyzed to investigate the dominant upper ocean processes controlling SST variability both north and south of 20°S.

3.1. Experiment design

Two sets of model experiments are conducted to elucidate the relative importance of surface heat flux and ocean dynamics for the interannual SST variation in the straus region. The first experiment uses the same wind stress as in the control experiment while the surface heat flux is the climatological annual cycle calculated from the output of the control experiment. This experiment is referred to as EX-1 hereafter. In EX-1, the interannual SST variation is driven by ocean dynamics through changes of currents and thermocline depth, while surface heat flux does not generate the interannual variation. Hence the SST variation generated by ocean dynamics can be isolated by the comparison with the control experiment. In the second experiment, the model was forced with the climatological wind stress (annual cycle) while the daily surface heat flux (that includes the interannual variation) from the control experiment is used (referred to as EX-2). The interannual variation of surface heat flux generates the SST variation in EX-2.

3.2. Results

Figure 7a shows SST anomalies for the area average 80°W-90°W, 10°S-20°S from EX-1 and the control experiment. These two time series are similar (rr=0.64), and the model is able to reproduce major El Nino events as in the control experiment. This indicates that a large portion of interannual SST variation associated with ENSO is driven through the ocean dynamics. SST anomalies for the same area average from EX-2 along with those from the control experiment are shown in Fig. 7b. The model is not able to reproduce the SST variation associated with El Nino (rr=0.05), showing that surface heat flux is not the primary driver of the interannual SST variation in this region. It should be noted that the annual mean SSTs of EX-1 (21.4°C) and EX-2 (20.8°C) are close to those of Reynolds SST and the control experiments (see Section 2.3).

Although the warming associated with major El Nino events are reproduced by EX-1, there are some discrepancies between EX-1 and the control experiment. For example, the timing of initial warming in early 1997 is not well reproduced by EX-1 whereas EX-2 generates a significant warming during this period. Also, other short timescale (4-9 months) variations such as those during 2000-2001 are not well reproduced by EX-1, while they are well reproduced by EX-2. This suggests that surface heat fluxes play an important role in SST variations in certain periods such as early 1997 as well as short timescale (4-9 months) variability.

Figure 8 shows temperature anomalies in the upper 300 m from the control experiment and EX-1. Overall, EX-1 is able to reproduce the vertical structure of temperature anomalies associated with major El Nino events. During the 1997/98 El Nino, the maximum anomaly is found near the surface, and the significant anomaly ($>0.5°$) extends to $\sim$300 m in both the control experiment and EX-1. The vertical

structure of the warm anomaly during 1982/83 El Nino is similar to those in the 1997/98 El Nino, but the anomalies are smaller. A subsurface maximum is found around 200 m during 1992 warm anomaly and during the 2003 cold anomaly in both experiments. The interannual variation of mixed layer depth in EX-1 is not similar to that in the control experiment, indicating that the interannual variation of surface heat flux significantly contributes to the mixed layer depth variation (not shown).

In order to examine the dominant upper ocean processes south of the IMET buoy, SST anomalies for the area average 80°W-90°W, 20°S-30°S from each experiment are also calculated (Fig. 9). The annual mean SST of EX-1 (20.0°C) and EX-2 (19.5°C) are close to those obtained from Reynolds SST and the control experiments. In this region, the relative importance of ocean dynamics and surface heat flux for determining SST variation is not as clear as that for the area north of 20°S based on the comparison of EX-1 and EX-2 with the control experiment. As discussed in Section 2.3.b, the SST variation in the control experiment is dominated by shorter time scale (∼4-9 months) variability, in which the ENSO signal is not evident. While EX-1 is not able to reproduce these 4-9 month SST variations, EX-2 is able to reproduce some of the short time scale SST variations especially after 1994 (rr=0.43 for the entire period, rr=0.61 after 1994). This suggests the importance of surface heat fluxes for controlling SST variations south of 20°S.

The results in this section as well as those in the previous section indicate that the IMET buoy site is located on the southern edge of the region dominated by ENSO, and that dominant processes which control the interannual SST variation are different north and south of 20°S in the stratus region. Accordingly, additional surface buoy measurements in locations both south and north of 20°S will help further improve our understanding of upper ocean processes associated with the interannual variation in the stratus cloud region.

4. Upper ocean processes

In the previous section, a series of OGCM experiments demonstrate that ocean dynamics play an important role in controlling the interannual variation of SST in the southeast Pacific north of 20°S. The interannual SST variation in EX-1 can be generated by both horizontal heat advection due to anomalous currents and vertical heat distribution due to vertical mixing through the variation of thermocline depth. In this section, a further analysis of the model output from EX-1 is performed to identify specific upper ocean processes that control the interannual SST in this region.

To examine the effect of horizontal heat advection on the SST, zonal ($\rho cu\frac{\partial T}{\partial x}$) and meridional ($\rho cv\frac{\partial T}{\partial x}$) heat advection in the mixed layer are computed from EX-1, where ρ is a water density, c is a specific heat, T is the average temperature in the mixed layer and u and v are average zonal and meridional velocities in the mixed layer, respectively. Figure 10a shows the time series of anomalies of 3 month average SST tendency, $-\rho cu\frac{\partial T}{\partial x}$, and $-\rho cv\frac{\partial T}{\partial y}$, at 80°W-90°W, 10°S-20°S. While both zonal and meridional heat advection are significantly correlated with SST tendency (Table 2), the correlation is much better for the meridional advection. In particular, large SST warming during major ENSO events is associated with positive (warming) anomalies of the meridional heat advection.

The variation of thermocline depth changes the temperature gradient below the mixed layer, that can affect the mixed layer temperature through the vertical mixing (entrainment). The vertical mixing term is also calculated from EX-1 to examine the impact of vertical heat distribution due to the mixing on SST. The term was computed during the experiment in which the difference of temperature profiles between before and after the mixing algorithm (KPP mixing scheme) was executed within each time step was saved (e.g., Shinoda and Hendon 2001). In this manner, accurate values of

heat gain or loss at each layer (or level) due solely to vertical mixing are obtained. Figure 10b shows anomalies in the vertical mixing term for EX-1. The time series of the vertical mixing term is not well correlated with SST tendency (Table 2), and thus the vertical mixing is not the dominant process in controlling the interannual SST variation in the model.

To further demonstrate how the meridional heat advection contributes to SST variability associated with ENSO in this region, the upper layer velocity and SST are described for specific periods when large SST changes are observed. Figure 11 shows SST and anomalous velocity in the upper 50 m near the IMET buoy site during August-December, 1997 when the strong warming associated with the ENSO event was found. Anomalous southward currents are evident in most of the areas north of 20°S. SST contour lines are mostly zonal, implying there is large meridional heat advection that brings warmer water from low latitudes southward.

The analysis of the model output in this section demonstrates the importance of horizontal heat advection associated with El Nino events for determining the interannual SST variation in the stratus cloud region north of 20°S. However, it should be noted that the vertical temperature gradient in the main thermocline is not well simulated by the model (Fig. 2), and that this model deficiency could possibly influence the heat budget calculation. For example, it is possible that more cold water could be entrained into the mixed layer by wind mixing if the thermocline in the model were much sharper. Thus efforts of model development which focus on the mixing parameterization below the mixed layer are desired for the further improvement of upper ocean heat budget estimates in this region.

5. Discussion and conclusions

Persistent stratus cloud decks in the southeast Pacific are important components of the complex air-sea-land coupled system, and their variations strongly impact on regional and global climate variability. The formation and maintenance of stratus clouds are strongly influenced by the variation of SST underneath. Accordingly, understanding upper ocean processes that control SST in this region is crucial for simulating stratus clouds and thus predicting regional and global climate.

This study investigates interannual variability of the upper ocean in the stratus cloud region and its relation to SST variability using ocean general circulation model (OGCM) experiments. The model was first forced with daily surface fluxes based on the NCEP reanalysis and satellite-derived surface shortwave and longwave radiation for the period of 1979-2004. These surface heat flux estimates and upper ocean temperature variation in the model are compared with those based on WHOI IMET buoy measurements at 85°W, 20°S. Gridded surface heat flux estimates agree well with those based on the buoy measurements. Also the seasonal evolution of mixed layer depth is reproduced by the model reasonably well. Then the model output is compared with long records of SST and SSH. The OGCM is able to well reproduce observed interannual SST and SSH variations in this region. North of the IMET site (80°W-90°W, 10°S-20°S), interannual SSH and SST variations are mostly associated with major El Nino events.

Additional model experiments were designed to examine the relative importance of ocean dynamics and surface heat fluxes for the interannual SST variation in this region. The first experiment uses daily wind stress while surface heat fluxes are the climatology. In the second experiment, the model was forced with climatological wind stress and daily surface heat fluxes. The first experiment is able to reproduce

interannual variation of SST north of 20°S, indicating that the ocean dynamics play an important role in controlling the SST variation in this region. Upper ocean heat budget is then computed from the first experiment to examine further details of upper ocean processes. The results suggest that the interannual SST variation in the stratus cloud region north of 20°S is mostly controlled by anomalous meridional heat advection associated with ENSO events.

A recent observational study (Colbo and Weller 2007) suggests the important role of eddies in maintaining the annual mean SST in the stratus region. Although the model used in this study is able to well reproduce observed interannual variations of the upper ocean, the model does not have sufficient horizontal resolution to fully generate submesoscale eddies. Hence the role of eddies in the interannual SST variation cannot be examined in these experiments. In recent years, eddy resolving models with fine horizontal resolution have been used in a variety of studies (e.g., Zamudio and Hogan 2008, Chang et al. 2008). However, most of these studies focus on time scales much shorter than interannual, or examine physical processes associated with the eddy-mean flow interaction and the behavior of eddies in idealized experiments (e.g., Berloff et al. 2007, Hyun and Hogan 2008). In addition, it is still uncertain how realistic the eddies in these models are especially with regard to their contributions to variability on interannual time scales. For example, it is difficult to verify the interannual variation of eddy activity in eddy-resolving models since the space and time coverage and resolution of in-situ and satellite observations are not yet sufficient for direct comparisons with these models. After the nature of eddies in fine resolution models is thoroughly examined, the importance of eddy activity for the interannual variation of SST in this region can be fully established.

While our results show that interannual variations of both SST and SSH in the model agree well with observations, there are some significant biases in net surface

heat and momentum fluxes as well as the general warm bias below the mixed layer. These biases might potentially affect some of the results in this study. In particular, the vertical temperature gradient in the main thermocline is not well simulated by the model, and this model deficiency could possibly influence the heat budget calculation. Hence, improvements of upper ocean mixing parameterization based on physical processes are needed to provide better estimates of upper ocean heat budget in the stratus cloud region.

For the purpose of better understanding and simulating how marine boundary layer cloud systems surrounding the Americas interact with the coupled ocean-atmosphere-land system, a new campaign: the VAMOS Ocean-Cloud-Atmosphere-Land Study (VOCALS) has been developed (http://www.eol.ucar.edu/projects/vocals/). A substantial amount of data in the upper ocean and atmospheric boundary layer in the stratus cloud region were recently collected during the VOCALS Regional Experiment (VOCALS REx; Wood et al. 2007). The results of the model experiments and diagnoses in this study will hopefully provide useful information for the analyses of the data obtained from VOCALS REx.

Acknowledgments

Data from the Stratus Ocean Reference Station were made available by Dr. Robert Weller of the Woods Hole Oceanographic Institution; these data were collected with support from the Pan American Climate Study and Climate Observation Programs of the Office of Global Programs, NOAA Office of Oceanic and Atmospheric Research, Grants NA17RJ1223, NA17RJ1224, and NA17RJ1225. TOPEX data are obtained from the Center for Space Research, University of Texas at Austin. This work was supported in part by a grant from the Computational and Information Systems Laboratory at NCAR. Constructive comments by two reviewers helped improve the original draft of this paper. Toshiaki Shinoda is supported by NSF Grants OCE-0453046 and ATM-0745897, and the 6.1 project Global Remote Littoral Forcing via Deep Water Pathways sponsored by the Office of Naval Research (ONR) under program element 601153N. Jialin Lin is supported by NSF Grant ATM-0745872 and NASA Modeling, Analysis and Prediction (MAP) Program.

References

Bleck, R., 2002: An oceanic general circulation model framed in Hybrid Isopycnic-Cartesian Coordinates, Ocean Modelling, 4, 55-88.

Berloff, P. P., A. C. Hogg, and W. Dewar, 2007:The Turbulent Oscillator: A Mechanism of Low-Frequency Variability of the Wind-Driven Ocean Gyres J. Phys. Oceanogr., 37, 2363-2386.

Chassignet, E. P., L. T. Smith, G. R. Haliwell, R. Bleck, 2003: North Atlantic simulations with Hybrid Coordinate Ocean Model (HYCOM): Impact of the vertical coordinate choice, reference density, and thermobaricity. J. Phys. Oceanogr., 33, 2504-2526.

Chang, Y., T. M. Ozgokmen, H. Peters, X. Xu, 2008: Numerical Simulation of the Red Sea Outflow Using HYCOM and Comparison with REDSOX Observations. JPO, 38, 337-358, doi: 10.1175/2007JPO3697.1

Colbo, K, and R. Weller, 2007: The variability and heat budget of the upper ocean under the Chile-Peru stratus. J. Mar. Res., 65, 607-637.

Fairall, C., E. F. Bradley, D. P. Rogers, J. B. Edson, G. S. Young, 1996: The TOGA COARE bulk flux algorithm J. Geophys. Res., 101, 3747-3764.

Fu, X., and B. Wang, 2001: A coupled modeling study of the seasonal cycle of the Pacific cold tongue, Part I: Simulation and sensitivity experiments. J. Climate, 14, 756-779.

Gordon, C. T., A. Rosati, and R. Gudgel, 2000: Tropical sensitivity of a coupled model to specified ISCCP low clouds. J. Climate, 13, 2239-2260.

Han, W., 2005: Origins and dynamics of the 90-day and 30-60 day variations in the equatorial Indian Ocean. J. Phys. Oceanogr. 708-728.

Han, W, T. Shinoda, L-L. Fu, and J. P. McCreary, 2006: Impact of atmospheric intraseasonal oscillations on the Indian Ocean dipole. J. Phys. Oceanogr., 36, 670-690.

Hyun, K.H. and P.J. Hogan, 2008: Topographic Effects on the Anticyclonic Vortex Evolution: A Modeling Study. Cont. Shelf Res., 28, 1246-1260

Kalnay, E., and Co-authors, 1996: The NCEP/NCAR 40-Year Reanalysis Project. Bull. Amer. Meteor. Soc., 77, 437-471.

Kessler, W. S., 2006: The circulation of the eastern tropical Pacific: A review. Procgress in Oceanography, 69, 181-217.

Klein, S. A., and D. L. Hartmann. 1993: The Seasonal Cycle of Low Stratiform Clouds. J. Climate, 6, 1587-1606.

Klein, S. A., D. L. Hartmann, and J. R. Norris, 1995: On the relationship among low cloud structure, sea surface temperature, and atmospheric circulation in the summertime northeast Pacific. J. Climate, 8, 1140-1155.

Large, W. G., and S. Pond, 1981: Open ocean momentum flux measurements in moderate to strong winds. J. Phys. Oceanogr., 11, 324-336.

Large, W. G., J. C. McWilliams and S. C. Doney, 1994: Oceanic vertical mixing: Review and a model with a nonlocal boundary layer parameterization. Rev. Geophys., 32, 363-403.

Levitus, S., R. Burgett, and T. P. Boyer, 1994:, World Ocean Atlas Volume 3: Salinity. NOAA Atlas, NESDIS 3, 99pp.

Levitus, S., and T. P. Boyer, 1994:, World Ocean Atlas Volume 4: Temperature. NOAA Atlas, NESDIS 3, 117pp.

Li, T., 1997: Air-sea interactions of relevance to the ITCZ: Analysis of coupled instabilities and experiments in a hybrid coupled GCM. J. Atmos. Sci., 54, 134-147.

Li, J.-L. F., M. Kohler, J. D. Farrara, and C. R. Mechoso, 2002: The impact of stratocumulus cloud radiative properties on surface heat fluxes simulated with a general circulation model. Mon. Wea. Rev., 1433-1441.

Lilly, D. K., 1968: Models of cloud-topped mixed layers under a strong inversion. Quart. J. Roy. Meteor. Soc., 94, 292-309.

Ma, C.-C., C. R. Mechoso, A. W. Robertson, and A. Arakawa, 1996: Peruvian stratus clouds and the tropical Pacific circulation: A coupled ocean-atmosphere GCM study. J. Climate, 9, 1635-1645.

Miller, R. L., 1997: Tropical thermostats and low cloud cover. J. Climate, 10, 409-440.

Norris, J. R., and C. B. Leovy, 1994: Interannual variability in stratiform cloudiness and sea surface temperature. J. Climate, 7, 1915-1925.

Philander, S. G. H., D. Gu, D. Halpern, G. Lambert, N.-C. Lau, T. Li, and R.C. Pacanowski, 1996: Why the ITCZ is mostly north of the equator. J. Climate, 9, 2958-2972.

Reynolds, R.W., N.A. Rayner, T.M. Smith, D.C. Stokes, and W. Wang, 2002: An improved in situ and satellite SST analysis for climate. J. Climate, 15, 1609-1625.

Schubert, W. H., 1976: Experiments with Lilly's cloud-topped model. J. Atmos. Sci., 33, 436-446.

Serra, Y. L., M. F. Cronin, G. N. Kiladis 2007: Sub-seasonal variance of surface meteorological parameters in buoy observations and reanalyses. Geophys. Res. Lett., 34, L12708, doi:10.1029/2007GL029506.

Shaji, C., C. Wang, G. R. Halliwell Jr., A. Wallcraft, 2005: Simulation of tropical Pacific and Atlantic Oceans using a HYbrid Coordinate Ocean Model. Ocean Modeling, 9, 253-282.

Shinoda, T., 2005: Impact of the diurnal cycle of solar radiation on intraseasonal SST variability in the western equatorial Pacific. J. Climate, 18, 2628-2636.

Shinoda, T., and H. H. Hendon 1998: Mixed layer modeling of intraseasonal variability in the tropical western Pacific and Indian Oceans. J. Climate, 11, 2668-2685.

Shinoda, T, and H. H. Hendon 2001: Upper ocean heat budget in response to the Madden Julian Oscillation in the western equatorial Pacific. J. Climate, 14, 4147-4165.

Shinoda, T., H. H. Hendon and J. Glick 1998: Intraseasonal variability of surface fluxes and sea surface temperature in the tropical western Pacific and Indian Ocean. J. Climate, 11, 1685-1702.

Shinoda, T, H. H. Hendon and J. Glick 1999: Intraseasonal surface fluxes in the tropical western Pacific and Indian Ocean from NCEP reanalyses. Mon. Wea. Rev., 127, 678-693.

Shinoda, T, P. E. Roundy, and G. E. Kiladis, 2008: Variability of intraseasonal Kelvin waves in the equatorial Pacific Ocean. J. Phys. Oceanogr., 38, 921-944.

Wood, R., C. Bretherton, B. Huebert, C. R. Mechoso, and R. Weller, 2007: The VAMOS Ocean-Cloud-Atmosphere-Land Study (VOCALS) Improving understanding, model simulations, and prediction of the Southeast Pacific Climate System. Program documents and information can be found at www.eol.ucar.edu/projects/vocals/

Xie, P., and P.A. Arkin, 1997: Global precipitation: A 17-year monthly analysis based on gauge observations, satellite estimates, and numerical model outputs. Bull. Amer. Meteor. Soc., 78, 2539 - 2558.

Xie, S.-P., 2004: The shape of continents, air-sea interaction, and the rising branch of the Hadley circulation. In The Hadley Circulation: Past, Present and Future, H. F. Diaz and R. S. Bradley (eds.), Kluwer Academic Publishers, Dordrecht.

Xu, H, S-P. Xie, and Y. Wang, 2005: Subseasonal Variability of the Southeast Pacific Stratus Cloud Deck. J. Climate, 18, 131-142.

Yu, J.-Y. and C. R. Mechoso, 1999: Links between annual variations of Peruvian stratocumulus clouds and of SST in the eastern equatorial Pacific. J. Climate, 12, 3305-3318.

Yu, Z., and P. Schopf, 1997: Vertical eddy mixing in the tropical upper ocean: Its influence on zonal currents. J. Phys. Oceanogr., 27, 1447-1458.

Zamudio, L., P. J. Hogan, 2008: Nesting the Gulf of Mexico in Atlantic HYCOM: Oceanographic processes generated by Hurricane Ivan. Ocean Modelling, 21, 106-12.

Zhang, Y., W. Rossow, and coauthors, 2004: Calculation of radiative flux profiles from the surface to top-of-atmosphere based on ISCCP and other global data

sets: refinements of the radiative transfer model and the input data. J. Geophys. Res., 109, D19105, doi:10.1029/2003JD004457.

Table captions

Table 1: Means, correlation coefficients and rms differences between surface fluxes estimated from IMET buoy data and gridded data.

Table 2: Correlation coefficients between SST tendency, zonal and meridional heat advection and vertical mixing in the mixed layer from EX-1.

Table 1: Means, correlation coefficients and rms differences between surface fluxes estimated from IMET buoy data and gridded data.

Surface flux	Mean		Correlation	Rms difference
	IMET	Gridded		
Shortwave radiation	187 W/m^2	184 W/m^2	0.80	29 W/m^2
Net surface heat flux	40 W/m^2	14 W/m^2	0.81	46 W/m^2
Zonal wind stress	-0.057 N/m^2	-0.073 N/m^2	0.86	0.020 N/m^2
Meridional wind stress	0.040 N/m^2	0.065 N/m^2	0.83	0.026 N/m^2

Table 2: Correlation coefficients between SST tendency, zonal and meridional heat advection and vertical mixing in the mixed layer from EX-1

SST tendency vs. Zonal heat advection	0.33
SST tendency vs. Meridional heat advection	0.60
SST tendency vs. Vertical mixing	0.19

Figure captions

Figure 1: (a) Time series of daily mean shortwave radiation from WHOI IMET measurements (solid line) and ISCCP-FD (dashed line) during 20 October 2001 - 21 October 2002. (b) Time series of daily mean net surface heat flux from WHOI IMET measurements (solid line) and gridded estimates used in the model integration (dashed line) during 20 October 2001 - 21 October 2002. (c) Time series of daily mean zonal wind stress from WHOI IMET measurements (solid line) and that based on the NCEP/NCAR reanalysis (dashed line). (d) Same as (c) except for the meridional wind stress.

Figure 2: (a) Daily mean temperature of upper 250 m during 20 October 2001 - 18 October 2002 from WHOI IMET measurements. The contour interval is 1°C. A 5-day running mean is applied to the time series. (b) Temperature (3-day interval) of upper 250 m during 20 October 2001 - 18 October 2002 from the control experiment. The contour interval is 1°C.

Figure 3:(a) Time series of mixed layer depth from WHOI IMET measurements (solid line) and from the control experiment (long dashed line) and SST from WHOI IMET measurements (short dashed line) and from the control experiment (dotted line) during 20 October 2001 - 21 October 2002. A 5-day running mean is applied to the time series of mixed layer depth from IMET measurements. (b) Time series of heat content in the upper 50 m from WHOI IMET measurements (solid line) and the control experiment (long dashed line) and heat content in the upper 200 m from WHOI IMET measurements (short dashed line) and the control experiment (dotted line). The ordinate on the left (right) side of the panel is for the upper 50 m (200 m) heat

content.

Figure 4: (a) Monthly mean SST anomalies at 85°W, 20°S from the control experiment (open circle) and Reynolds SST (closed circle). (b) Same as (a) except for SST anomalies averaged over the area 90°W-80°W, 10°S-20°S. (c) Same as (a) except for SST anomalies averaged over the area 90°W-80°W, 20°S-30°S.

Figure 5: (a) Monthly mean SST anomalies in November, 1997 from Reynolds SST. "X" in the map indicates the IMET buoy site. (b) Same as (a) except for January, 1992.

Figure 6: (a) Monthly mean SSH anomalies at 85°W, 20°S from the control experiment (open circle) and TOPEX altimeter measurements (closed circle). (b) Same as (a) except for SSH anomalies averaged over the area 90°W-80°W, 10°S-20°S. (c) Same as (a) except for SSH anomalies averaged over the area 90°W-80°W, 20°S-30°S.

Figure 7: (a) Monthly mean SST anomalies averaged over the area 90°W-80°W, 10°S-20°S from the control experiment (solid line) and EX-1 (dashed line). (b) Monthly mean SST anomalies averaged over the area 90°W-80°W, 10°S-20°S from the control experiment (solid line) and EX-2 (dashed line).

Figure 8: (a) Monthly mean temperature anomalies of upper 300 m averaged over the area 90°W-80°W, 10°S-20°S from the control experiment. The contour interval is 0.5°C. Dashed contours indicate negative values. (b) Same as (a) except for EX-1.

Figure 9: Same as Fig. 7 except for the area 90°W-80°W, 20°S-30°S.

Figure 10: (a) Anomalies of 3-month mean SST tendency (solid line), zonal (dotted line) and meridional (dashed line) heat advection in the mixed layer from EX-1. A 1-2-1 smoothing is applied for the time series. ρc is multiplied to the SST tendency term. (b) Anomalies of 3-month mean SST tendency (solid line) and vertical mixing term (dashed line) in the mixed layer from EX-1. A 1-2-1 smoothing is applied to the time series.

Figure 11: Current anomalies (m/s; arrows) in the upper 50 m and SST (shading) during August-December 1997 from EX-1.

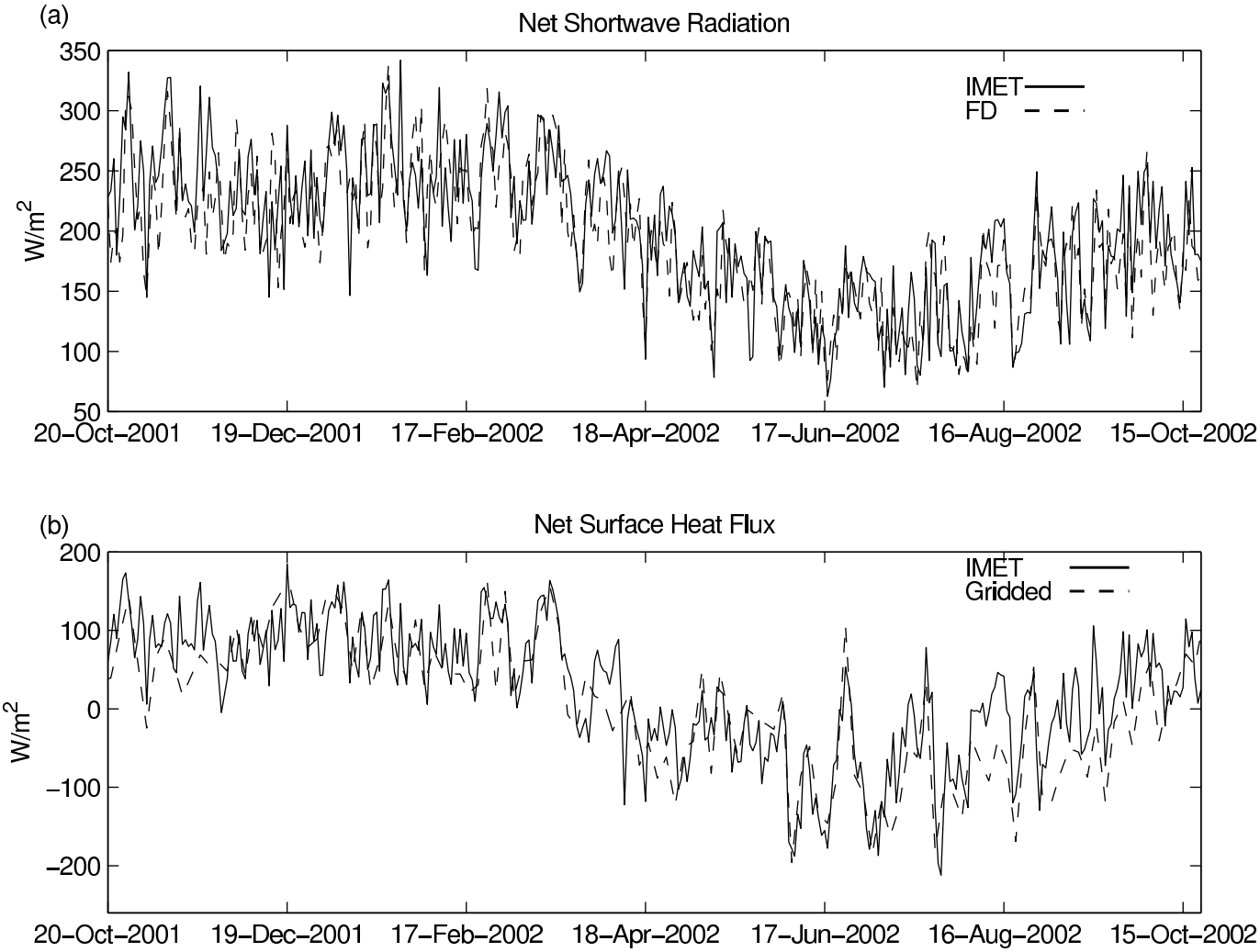

Figure 1:(a) Time series of daily mean shortwave radiation from WHOI IMET measurements (solid line) and ISCCP-FD (dashed line) during 20 October 2001 - 21 October 2002. (b) Time series of daily mean net surface heat flux from WHOI IMET measurements (solid line) and gridded estimates used in the model integration (dashed line) during 20 October 2001 - 21 October 2002. (c) Time series of daily mean zonal wind stress from WHOI IMET measurements (solid line) and that based on the NCEP/NCAR reanalysis (dashed line). (d) Same as (c) except for the meridional wind stress.

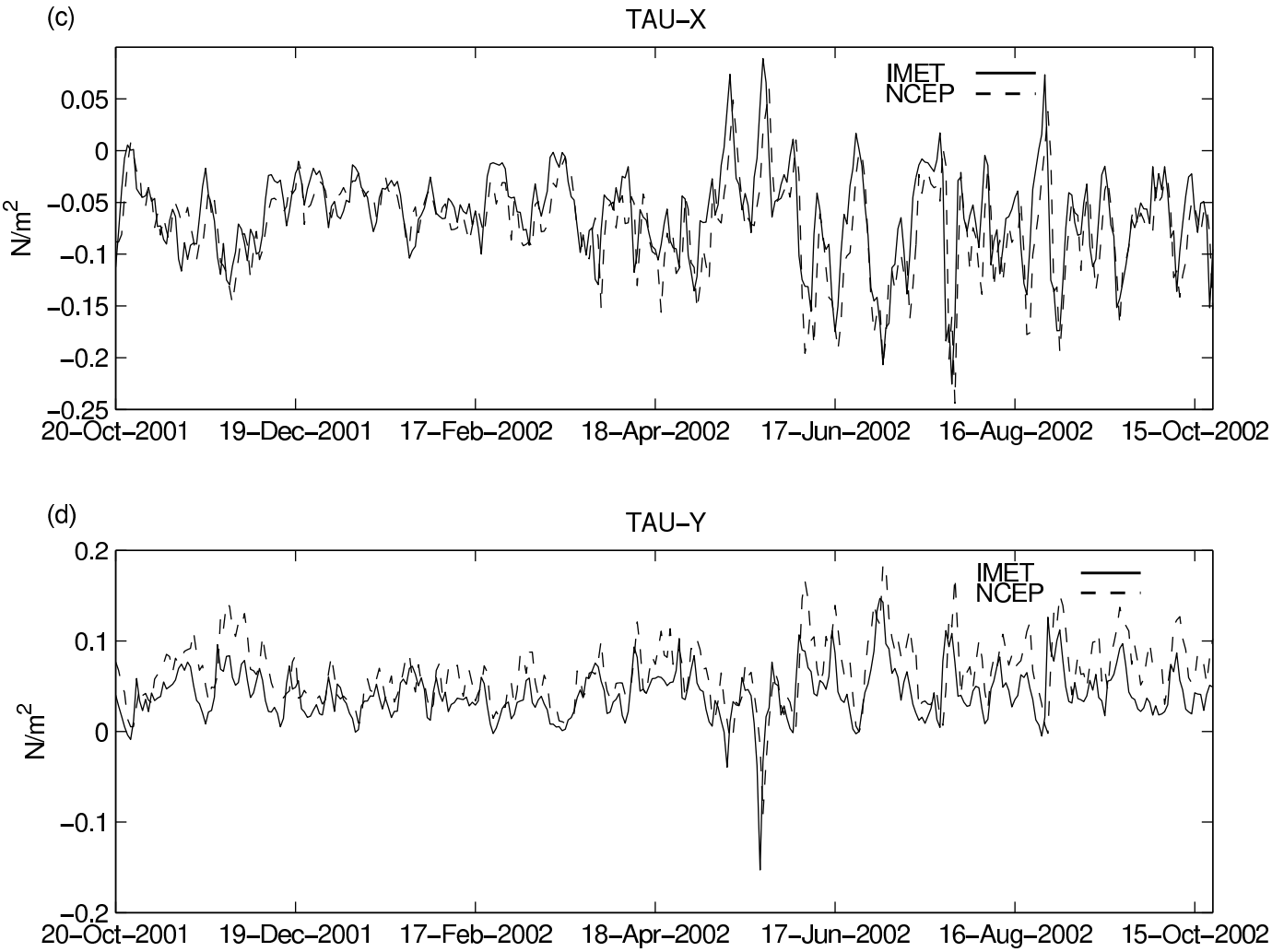

Figure 1 (continue)

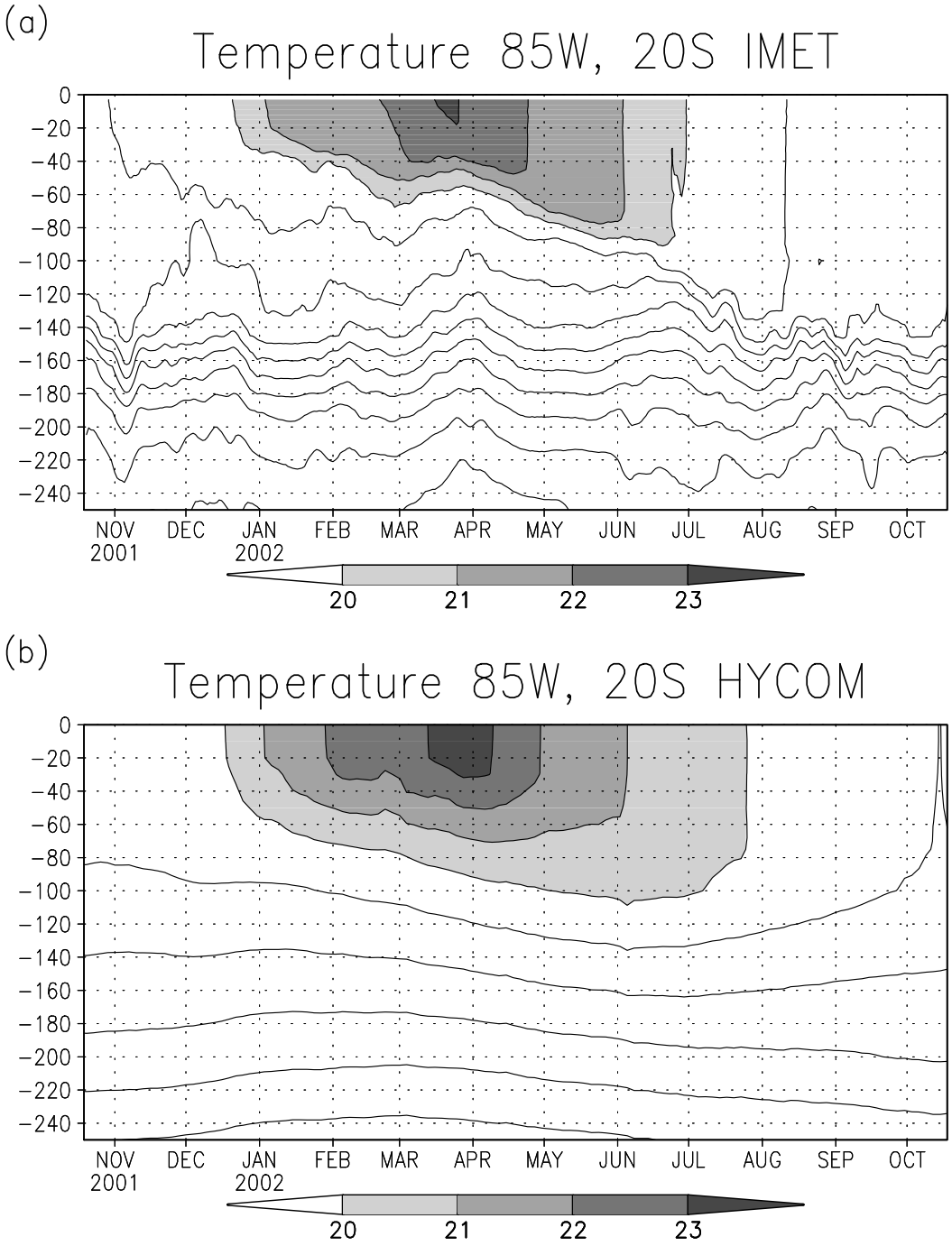

Figure 2: (a) Daily mean temperature of upper 250 m during 20 October 2001 - 18 October 2002 from WHOI IMET measurements. The contour interval is 1°C. A 5-day running mean is applied to the time series. (b) Temperature (3-day interval) of upper 250 m during 20 October 2001 - 18 October 2002 from the control experiment. The contour interval is 1°C.

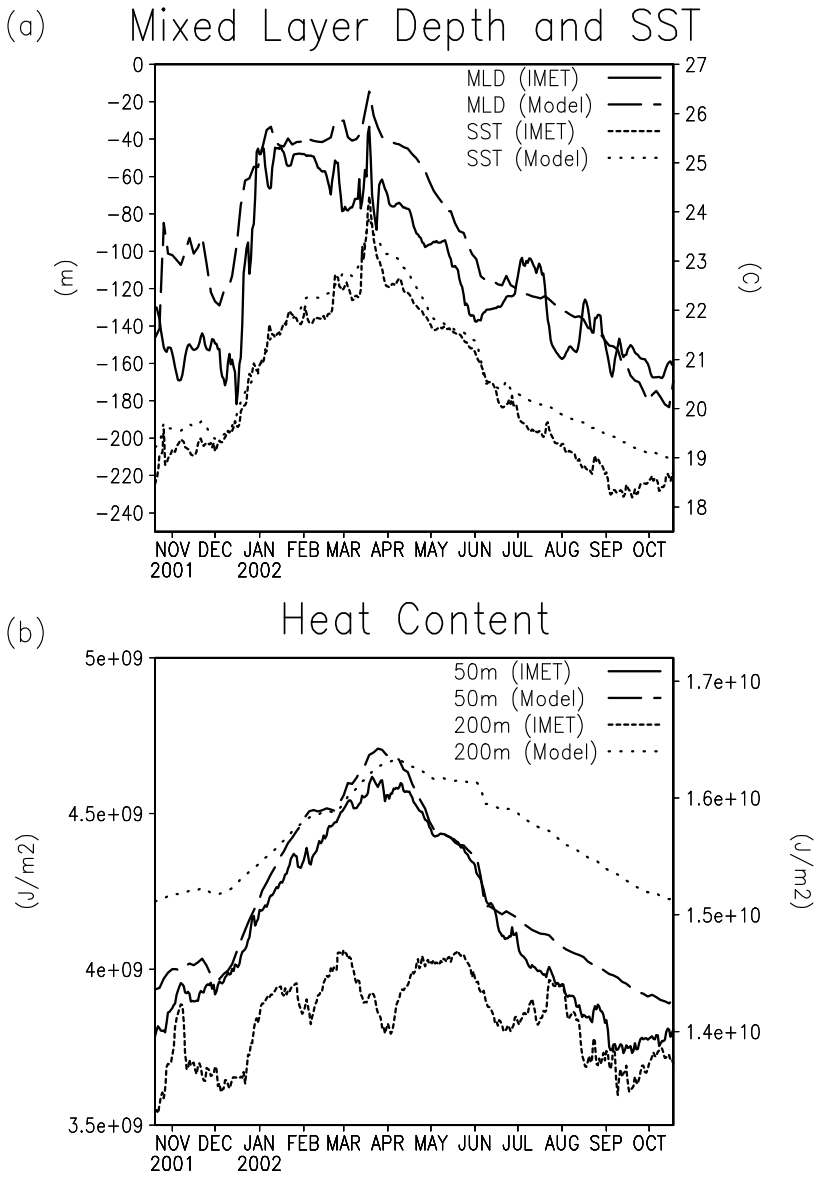

Figure 3:(a) Time series of mixed layer depth from WHOI IMET measurements (solid line) and from the control experiment (long dashed line) and SST from WHOI IMET measurements (short dahesd line) and from the control experiment (dotted line) during 20 October 2001 - 21 October 2002. A 5-day running mean is applied to the time series of mixed layer depth from IMET measurements. (b) Time series of heat content in the upper 50 m from WHOI IMET measurements (solid line) and the control experiment (long dashed line) and heat content in the upper 200 m from WHOI IMET measurements (short dashed line) and the control experiment (dotted line). The ordinate on the left (right) side of the panel is for the upper 50 m (200 m) heat content.

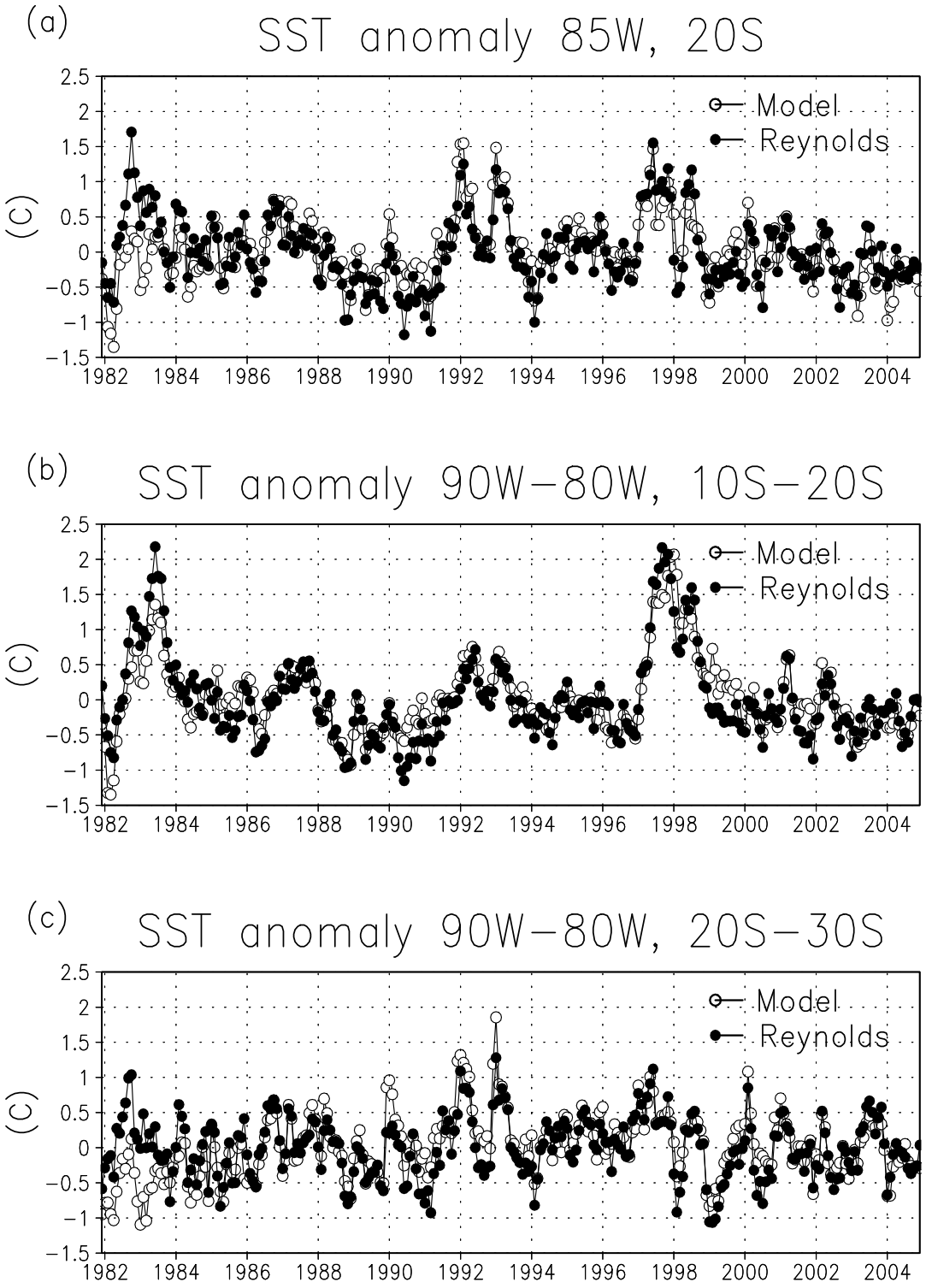

Figure 4: (a) Monthly mean SST anomalies at 85°W, 20°S from the control experiment (open circle) and Reynolds SST (closed circle). (b) Same as (a) except for SST anomalies averaged over the area 90°W-80°W, 10°S-20°S. (c) Same as (a) except for SST anomalies averaged over the area 90°W-80°W, 20°S-30°S.

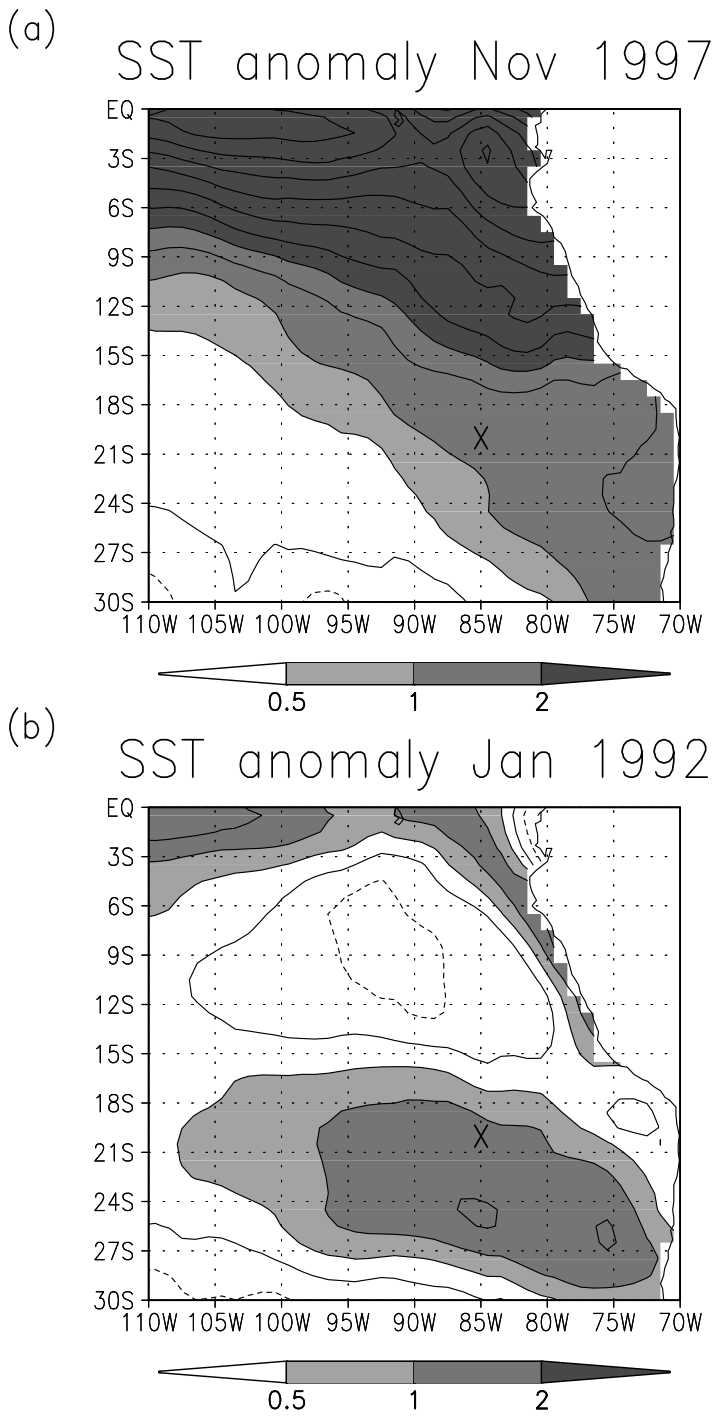

Figure 5: (a) Monthly mean SST anomalies in November, 1997 from Reynolds SST. "X" in the map indicates the IMET buoy site. (b) Same as (a) except for January, 1992.

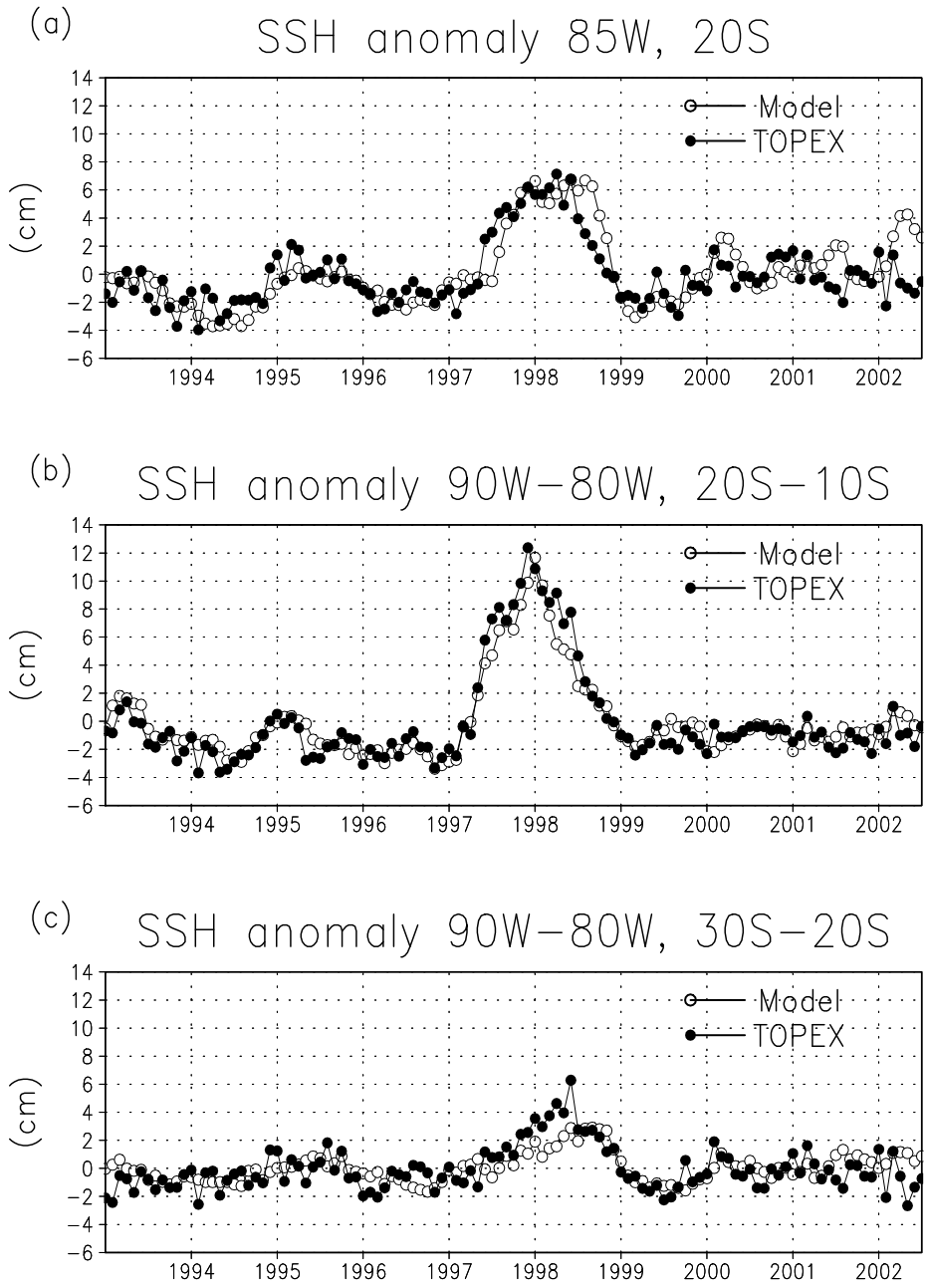

Figure 6: (a) Monthly mean SSH anomalies at 85°W, 20°S from the control experiment (open circle) and TOPEX altimeter measurements (closed circle). (b) Same as (a) except for SSH anomalies averaged over the area 90°W-80°W, 10°S-20°S. (b) Same as (a) except for SSH anomalies averaged over the area 90°W-80°W, 20°S-30°S.

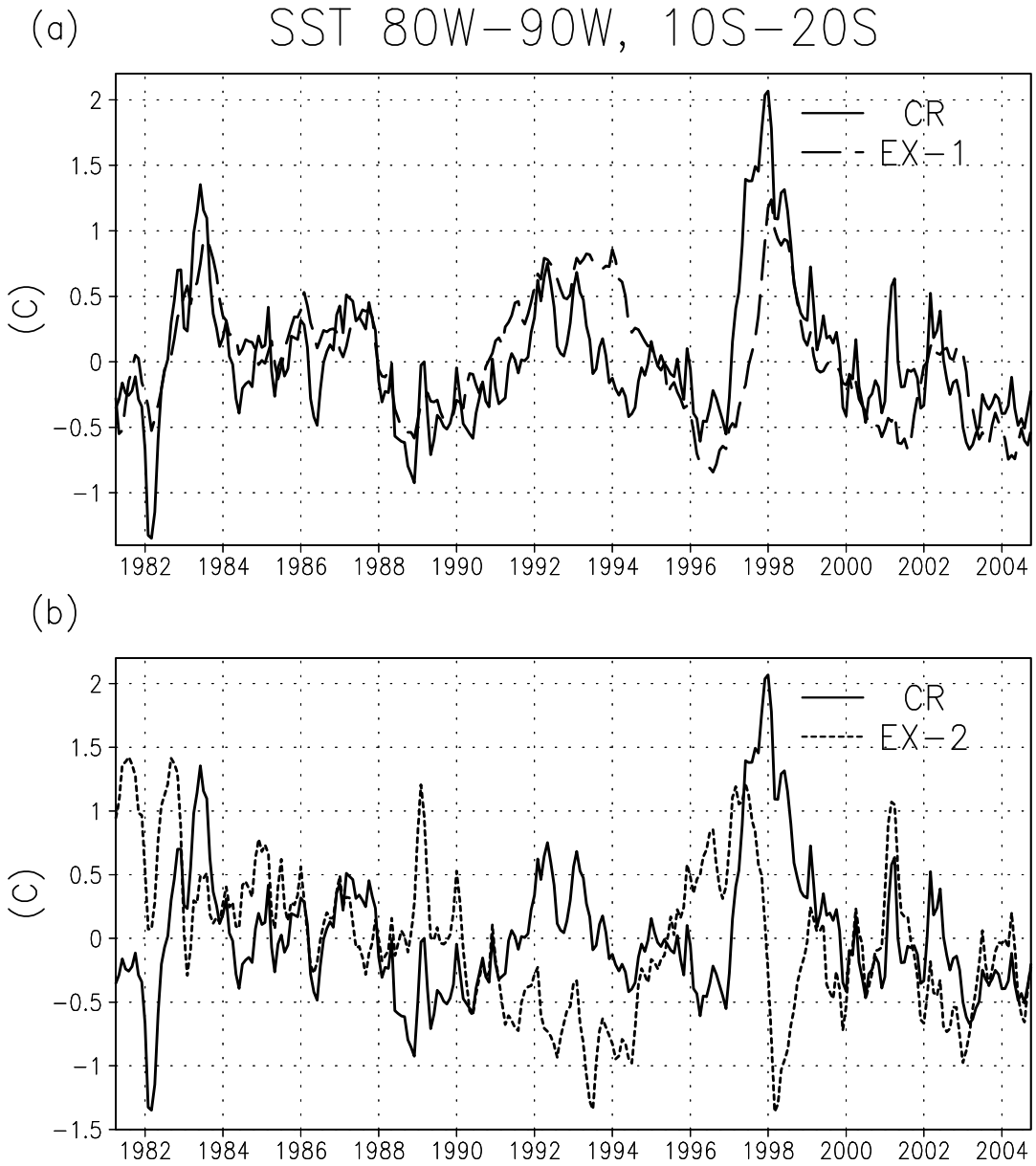

Figure 7: (a) Monthly mean SST anomalies averaged over the area 90°W-80°W, 10°S-20°S from the control experiment (solid line) and EX-1 (dashed line). (b) Monthly mean SST anomalies averaged over the area 90°W-80°W, 10°S-20°S from the control experiment (solid line) and EX-2 (dashed line).

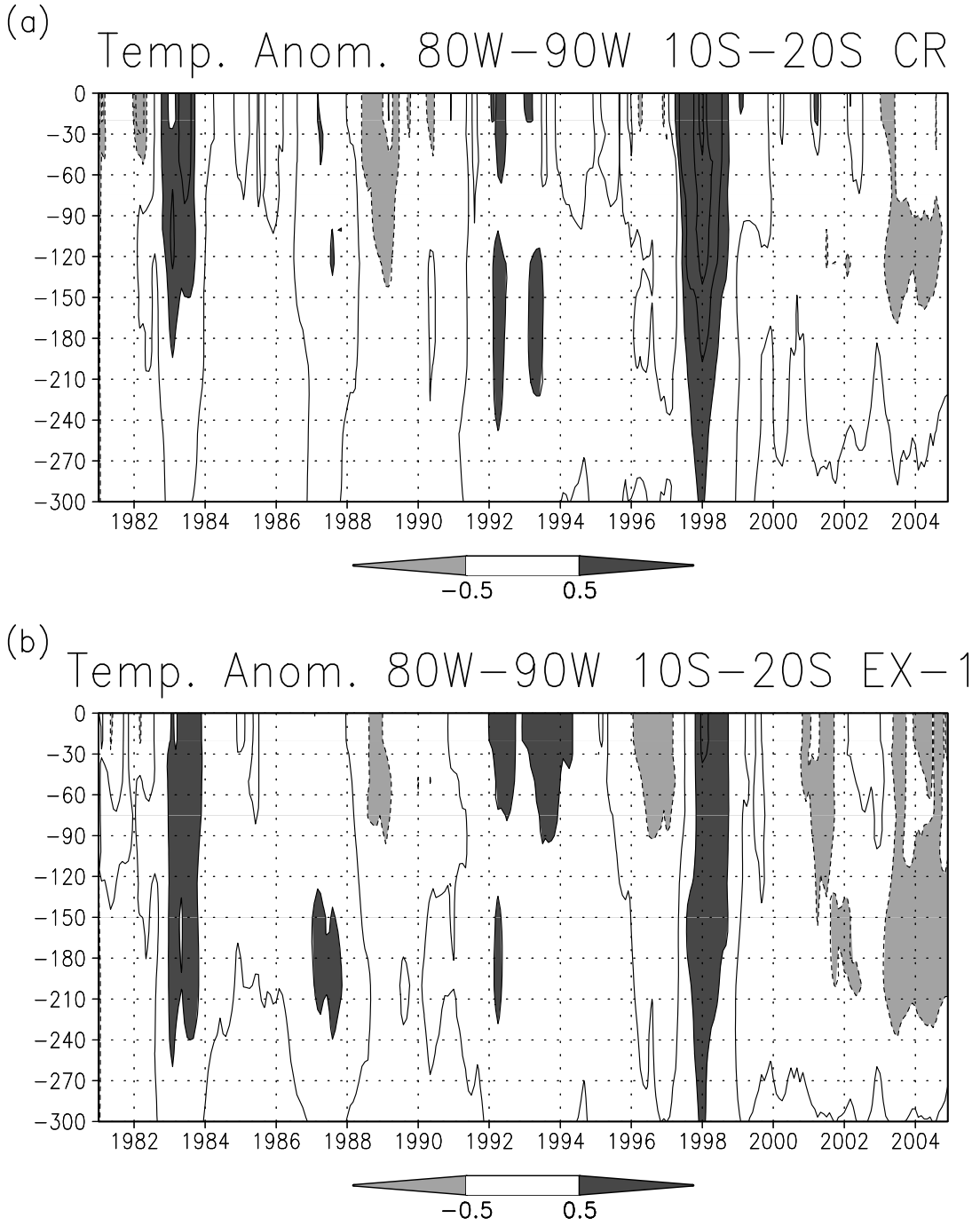

Figure 8: (a) Monthly mean temperature anomalies of upper 300 m averaged over the area 90°W-80°W, 10°S-20°S from the control experiment. The contour interval is 0.5°C. Dashed contours indicate negative values. (b) Same as (a) except for EX-1.

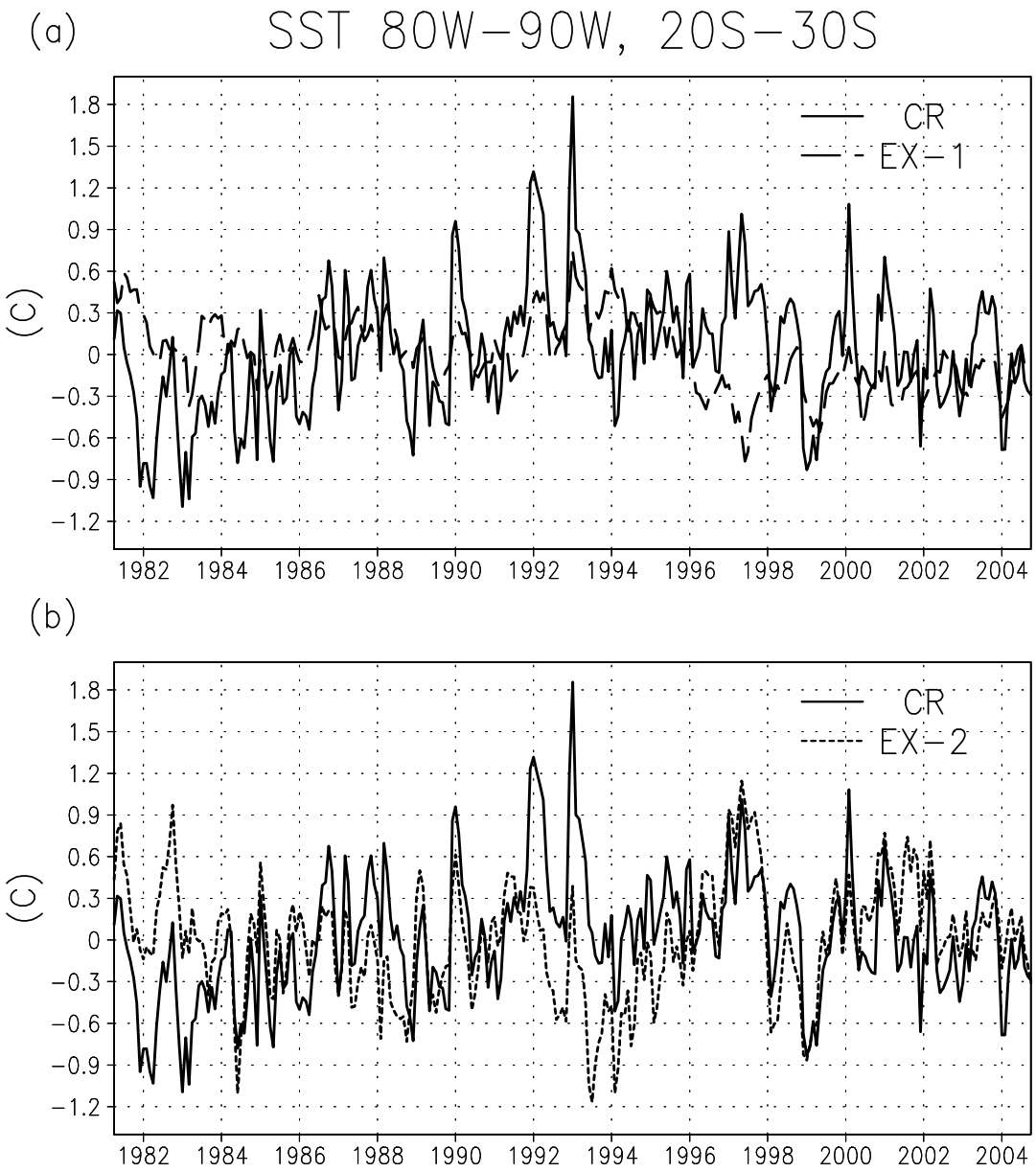

Figure 9: Same as Fig. 7 except for the area 90°W-80°W, 20°S-30°S.

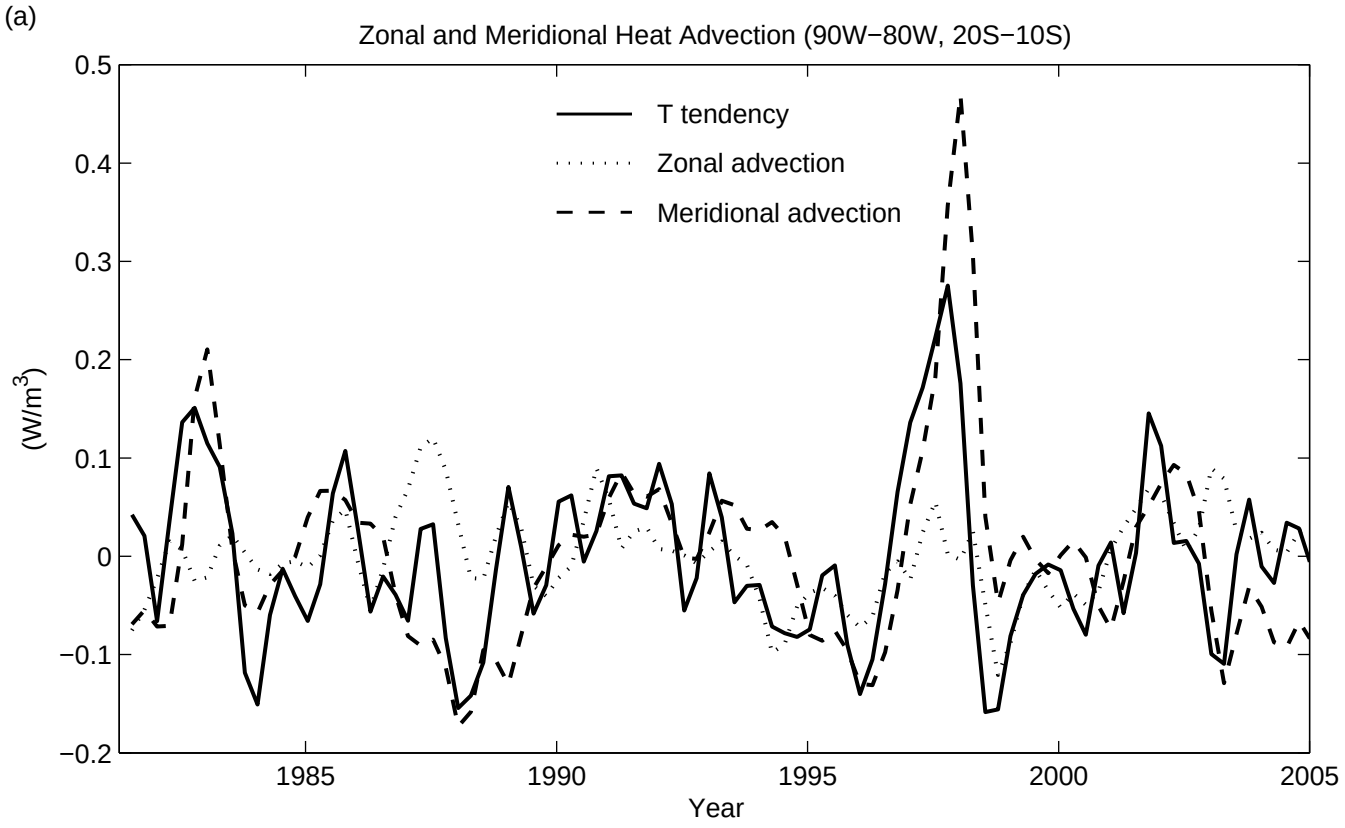

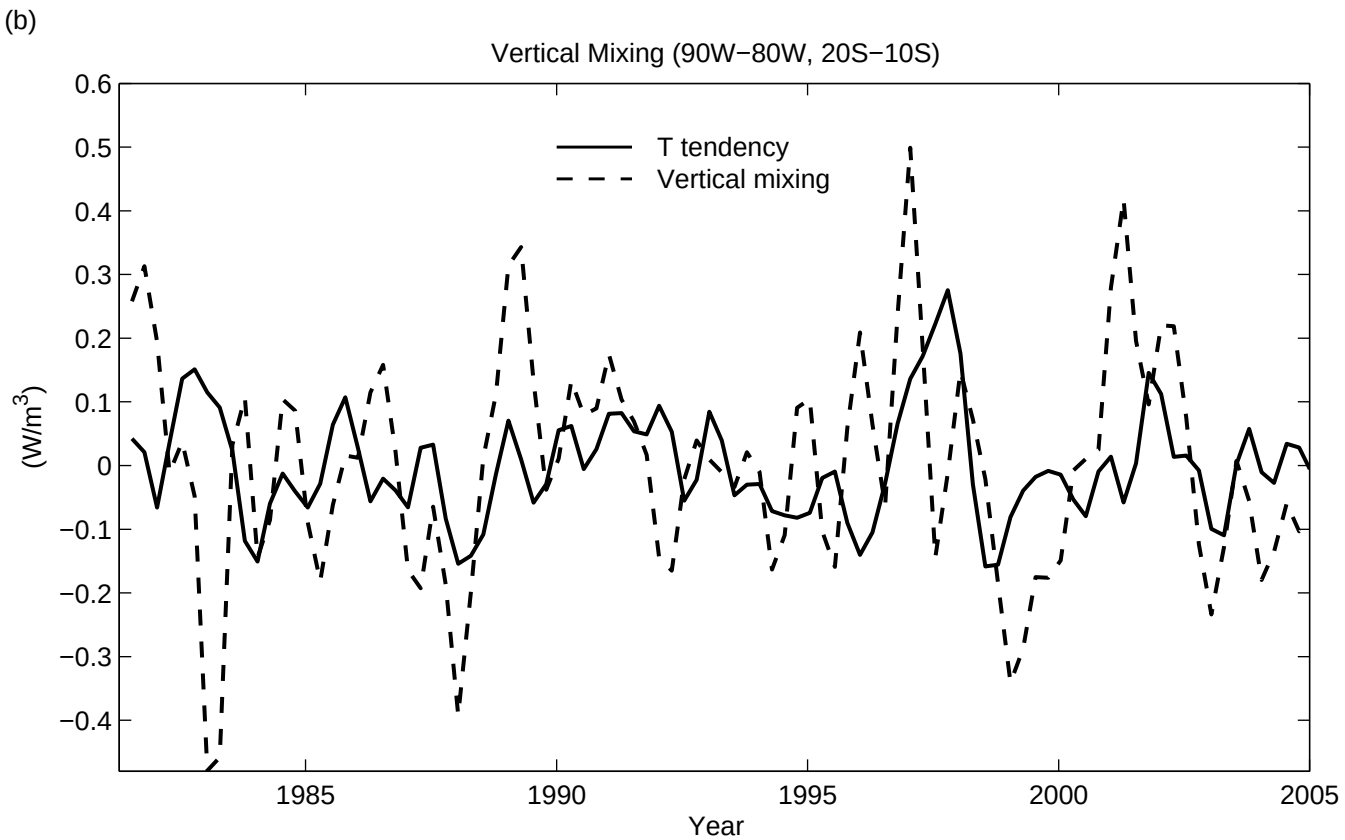

Figure 10 (a) Anomalies of 3-month mean SST tendency (solid line), zonal (dotted line) and meridional (dashed line) heat advection in the mixed layer from EX-1. A 1-2-1 smoothing is applied for the time series. ρc is multiplied to the SST tendency term. (b) Anomalies of 3-month mean SST tendency (solid line) and vertical mixing term (dashed line) in the mixed layer from EX-1. A 1-2-1 smoothing is applied to the time series.

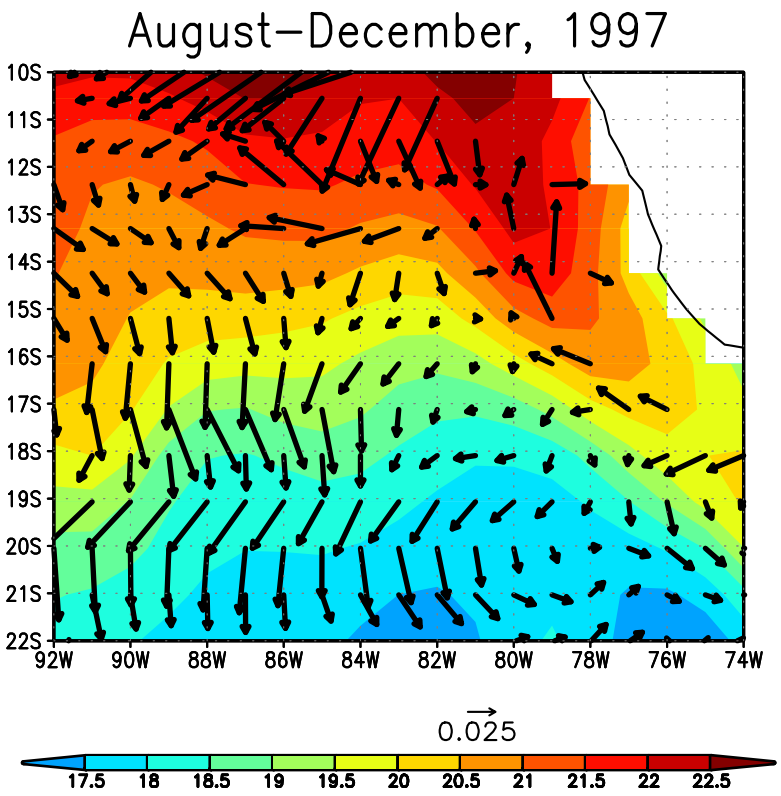

Figure 11: Current anomalies (m/s; arrows) in the upper 50 m and SST (shading) during August-December 1997 from EX-1.